constructed from only one slice at the largest cut surface of tumors, which did not allow the evaluation of three-dimensional (3D) CT numbers.

On the other hand, multidetector CT scanning, which is now widely used in routine clinical practice, offers high scan speed and enables volume data for pulmonary nodules to be obtained with thin sections. In this study, we performed a 3D analysis of the CT number from volume data obtained with multidetector CT scanning and investigated the optimal parameters for differentiating among AAH, BAC, and adenocarcinoma.

Materials and Methods

Eligibility

The study protocol for examining CT numbers on HRCT scans in patients with GGO nodules was approved by the ethics committee of Kumamoto University Hospital in May 2005. Informed consent was obtained from all patients after they had a discussion of the risks and benefits of the study with their surgeons.

Patients

Between June 2005 and December 2006, 38 patients with GGO nodules prospectively underwent HRCT scans, and the CT number obtained by 3D computerized quantification was examined. IV contrast material was not used for this examination. Of these, 43 GGO nodules in 33 patients were resected and examined pathologically, and were included in this study (Table 1). The number of the lesions resected per patient was one in 27 patients, two in 3 patients, three in 2 patients, and four in 1 patient. All of the lesions were < 3 cm in size and showed GGO with a small solid component. The histologic diagnosis was AAH in 10 lesions, BAC in 21 lesions, and adenocarcinoma in 12 lesions. The mean size was 0.8 cm (range, 0.6 to 1.0 cm) in AAH lesions, 1.4 cm (range, 0.5 to 2.4 cm) in BAC lesions, and 1.8 cm (range, 1.2 to 2.5 cm) in adenocarcinoma lesions. All of the 12 adenocarcinoma lesions were histologically well differentiated. All 21 BAC lesions and all 12 adenocarcinoma lesions were T1N0M0. The histologic criteria for AAH, BAC, and adenocarcinoma were based on the 1999 World Health Organization histologic classification.[9,10] To check stromal, vascular, and pleural invasion, we routinely performed Victoria blue staining.

Table 1—*Clinicopathologic Characteristics of Patients With GGO Nodules*

Characteristics	Values
Age, yr	
Mean	68
Range	55–79
Sex, No.	
Male	16
Female	17
Resected lesions, No.	
1	27
2	3
3	2
4	1
Smoking status, No.	
Positive	14
Negative	19
Surgical procedure, No.	
Lobectomy	5
Segmentectomy	24
Wedge resection	4
Total	33

Segmentation of GGO Nodules by a Computerized Automated Diagnosis System

Volume scans of the nodules were performed using a four-detector CT scanner (LightSpeed QX/I; GE Medical Systems; Milwaukee, WI). The scanning parameters were as follows: detector collimation, 4 × 1.25 mm; helical pitch, 0.75; section thickness, 1.25 mm; section interval, 1.25 mm; rotation time, 0.8 s; tube voltage, 120 kVp; and tube current, 160 to 200 mA. The segmentation of GGO nodules was conducted using a computerized automated diagnosis (CAD) system developed in-house, which has been reported previously.[11,12] First, one radiologist (K.A.) specified the region of interest on a section that included the target GGO nodule (Fig 1). The threshold CT number between GGO nodules and surrounding normal lung tissue was set at −700 to −800 Hounsfield units (HU). The CAD system automatically identified the GGO nodules in all x-axis, y-axis, and z-axis directions from the surrounding normal lung tissue. The elimination of normal structures within or around the nodule, such as vessels and bronchioli, was performed using several image-processing techniques,.[13,14] Therefore, the nodule was identified as the lesion area without vessels and bronchioli.

Analysis of CT Number of GGO Nodules

CT numbers of nodules were tallied up three-dimensionally with a computer workstation (CELSIUS; Fujitsu; Tokyo, Japan) with dual 3.0-GHz processors (Xeon; Intel; Santa Clara, CA). A CT number histogram was generated with the class interval of 8 HU. We quantified the following variables: (1) the CT number histogram pattern; (2) the CT number at the highest peak on the histogram; (3) the mean CT number; and (4) the CT numbers at the 5th, 10th, 25th, 50th, 75th, 90th, and 95th percentiles (*eg*, a 25th percentile value means a CT number of the 25% of the pixels calculated from the pixel with the minimum CT number, and a 50th percentile signifies the median CT number).

Evaluation by Receiver Operating Characteristic Curve

Optimum variables to differentiate among AAH, BAC, and adenocarcinoma were evaluated on receiver operating characteristic (ROC) curves using a statistical software package (SPSS; SPSS Inc; Chicago, IL).

*From the Departments of Thoracic Surgery (Drs. Ikeda, Mori, and Nomori) and Diagnostic Radiology (Drs. Awai, Kawanaka, and Yamashita), Graduate School of Medical Sciences, Kumamoto University, Honjo, Kumamoto, Japan.
The authors have reported to the ACCP that no significant conflicts of interest exist with any companies/organizations whose products or services may be discussed in this article.
Manuscript received March 29, 2007; revision accepted May 17, 2007.

Correspondence to: Hiroaki Nomori, MD, PhD, Department of Thoracic Surgery, Graduate School of Medical Sciences, Kumamoto University, 1-1-1 Honjo, Kumamoto 860-8556, Japan; e-mail: hnomori@qk9.so-net.ne.jp
DOI: 10.1378/chest.07-0793

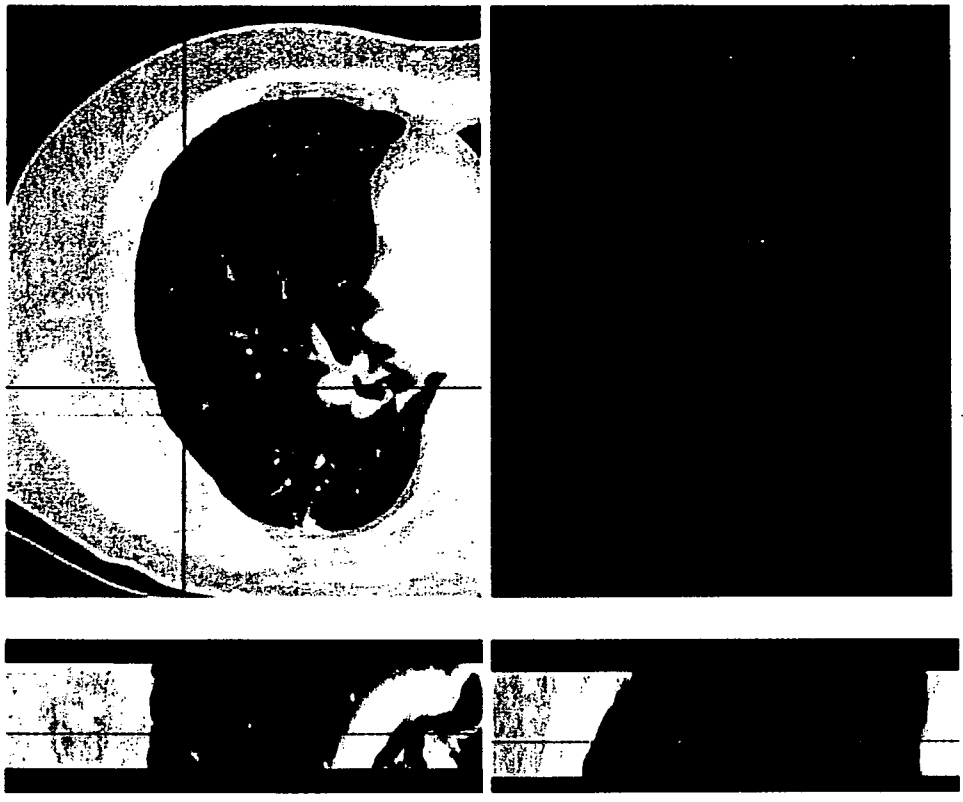

FIGURE 1. *Top left*: a GGO nodule segmented by a CAD system. *Top right*: 3D image of the GGO lesion segmented by the CAD system. *Bottom left*: coronal view of the lesion. *Bottom right*: sagittal view of the lesion.

Statistical Analysis

All values in the text and tables are given as the mean ± SD. Category data were compared using the Fisher exact test. The data for the CT number were analyzed for significance using the two-tailed Student *t* test. A Bonferroni test was used to determine significance for comparisons among the three parts. p Values of < 0.05 were accepted as significant.

RESULTS

The CT number histograms showed the following two patterns: one in which there was a peak at a low CT number zone (n = 30); and the other with two peaks, one each at the low and high CT number zones (n = 13) [Fig 2]. The low CT number zone ranged from −440 to −800 HU, and the high zone ranged from −24 to −96 HU. In the pattern with two peaks, the peak at the low CT number zone was usually higher than that at the high zone. While all of the 10 AAH lesions showed the one-peak pattern, 8 of the 21 BAC lesions (38%) and 5 of the 12 adenocarcinoma lesions (42%) showed the two-peak pattern (Table 2). There was no significant difference in histogram pattern between BAC and adenocarcinoma lesions.

Table 3 shows the area under the curve (AUC) on the ROC curve for each variable for differentiating among AAH, BAC, and adenocarcinoma lesions. For differentiating AAH from BAC or differentiating AAH from BAC and adenocarcinoma, a 75th percentile CT number showed the largest AUC, indicating the highest sensitivity and specificity. For differentiating adenocarcinoma from BAC or differentiating adenocarcinoma from BAC and AAH, the mean CT number showed the largest AUC. The ROC curve to differentiate between AAH and BAC with the 75th percentile CT number showed the cutoff value to be −584 HU (Fig 3). The ROC curve to differentiate between adenocarcinoma and BAC with the mean CT number showed the cutoff value to be −472 HU (Fig 4). Figure 5 shows the distribution of the 75th percentile CT number in AAH, BAC, and adenocarcinoma. The mean values of the 75th percentile of AAH, BAC, and adenocarcinoma were −609 ± 45, −450 ± 147, and −319 ± 97 HU, respectively, which shows a significant difference between AAH and BAC and between BAC and adenocarcinoma ($p < 0.05$). Figure 6 shows the distribution of mean CT numbers for AAH, BAC, and adenocarcinoma. The mean values of the mean CT

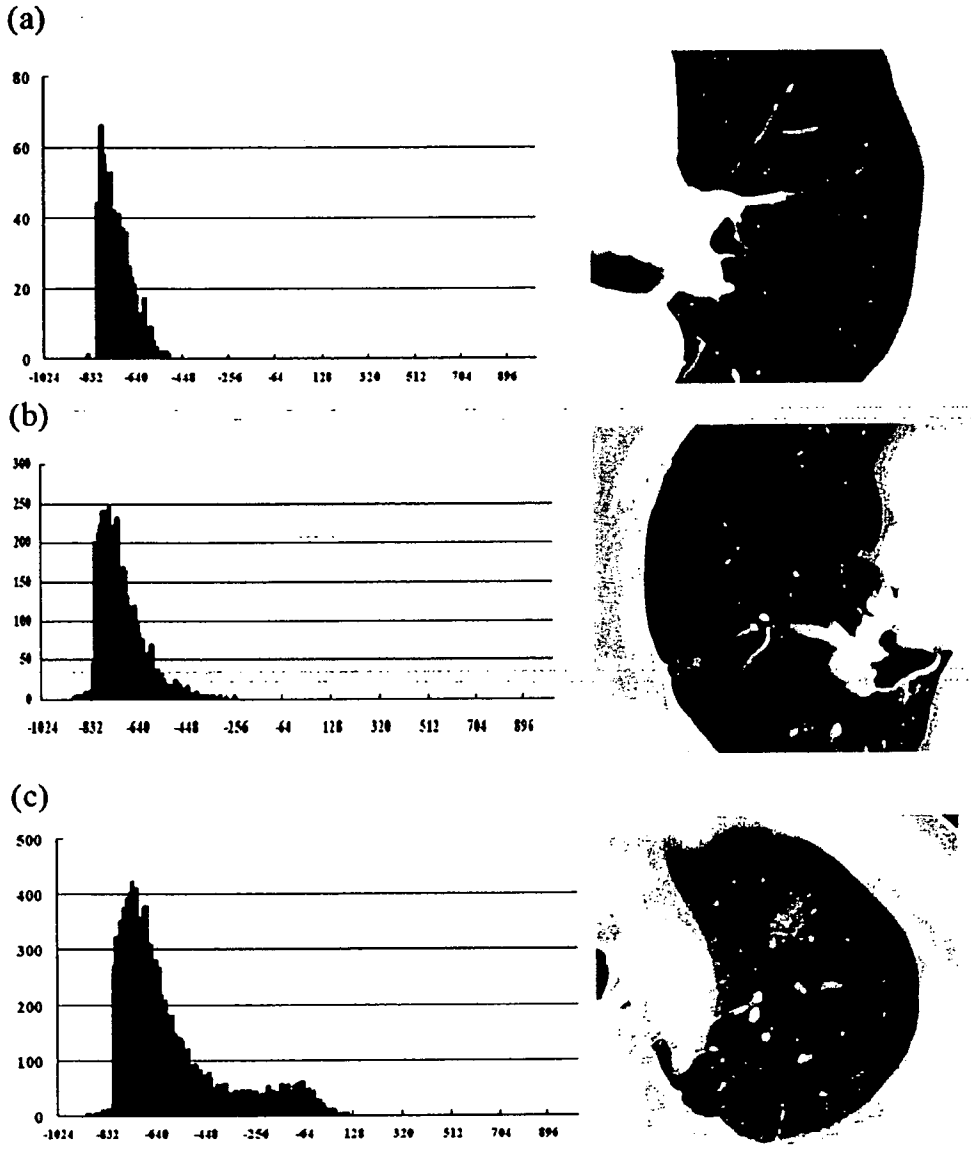

FIGURE 2. CT number histogram and CT image. The vertical axis in each histogram shows the number of pixels in the lesion. The horizontal axis shows the CT numbers, for each of which the class interval was 8 HU. *Top, a*: AAH with one peak on the histogram. *Middle, b*: BAC with one peak on the histogram. *Bottom, c*: adenocarcinoma with two peaks on the histogram, showing a mixed solid component in a GGO lesion.

number for AAH, BAC, and adenocarcinoma were -660 ± 35, -556 ± 95, and -442 ± 99 HU, respectively, with a significant difference between AAH and BAC and between BAC and adenocarcinoma ($p < 0.01$).

Table 4 shows the result of differentiation between AAH and BAC with a cutoff value of -584 HU at the 75th percentile, for which the sensitivity was 0.9, the specificity was 0.76, and the accuracy was 0.81. Table 5 shows the result of differentiation

Table 2—*Patterns of CT Number Histogram in AAH, BAC, and Adenocarcinoma**

Histogram Pattern	AAH	BAC	Adenocarcinoma	Total
One peak	10	13	7	30
Two peaks	0	8	5	13
Total	10	21	12	43

*Data are presented as No.

Table 3—*AUC of ROC Curve for Differentiating Among AAH, BAC, and Adenocarcinoma**

Variables	AAH/BAC	AAH/BAC and Ad	Ad/BAC	Ad/BAC and AAH
Mean CT No.	0.810	0.879	0.810†	0.871†
Peak CT No.	0.829	0.831	0.615	0.692
5th percentile	0.788	0.803	0.704	0.745
10th percentile	0.800	0.814	0.722	0.759
25th percentile	0.817	0.855	0.750	0.805
50th percentile	0.829	0.883	0.794	0.853
75th percentile	0.852†	0.906†	0.732	0.819
90th percentile	0.831	0.892	0.677	0.781
95th percentile	0.848	0.879	0.615	0.765

*Ad = adenocarcinoma.
†The largest AUC.

between adenocarcinoma and BAC with a cutoff value of −472 HU at the mean CT number, with a sensitivity of 0.75, a specificity of 0.81, and an accuracy of 0.79.

Discussion

This study showed that the 75th percentile CT number of GGO lesions was the optimal CT number variable for differentiating between AAH and BAC or AAH and another histology (*ie*, BAC and adenocarcinoma). We previously reported that, by examining the CT numbers on two-dimensional images, the peak CT histogram number was superior to the mean CT number for differentiating between AAH and BAC.[5] Because this study examined the CT numbers from 3D computerized quantification and investigated a many more parameters, including several percentile CT numbers, we believe that the data from this study is more precise than that from our previous study. The reason why the 75th percentile was superior to the peak CT number on the histogram could be the following: (1) because BAC frequently shows an AAH-like component at the peripheral site, its peak CT number on the histogram may sometimes be similar to that of AAH, especially in BAC with a broad AAH-like component; (2) because the 75th percentile indicates the high CT number zone within the lesions, differences in the thickening of alveolar septa and cellularity between AAH and BAC may be revealed.

However, 1 of the 10 AAH lesions and 5 of the 21

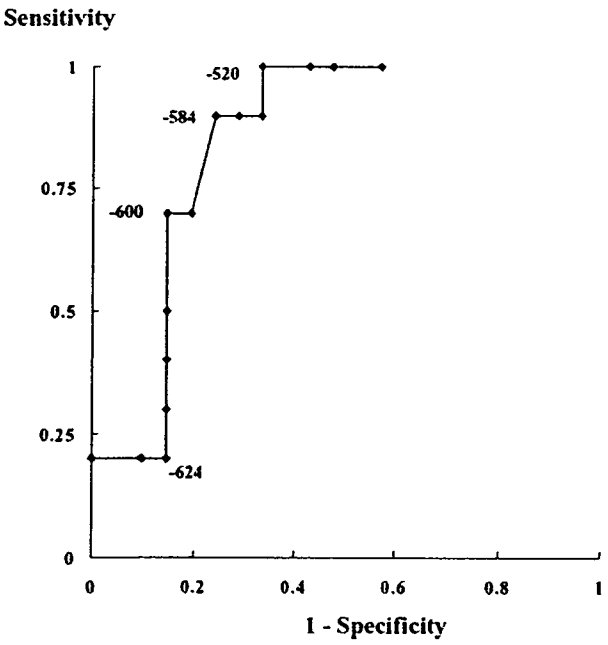

FIGURE 3. ROC curve of the CT number of the 75th percentile for differentiation between AAH and BAC, showing the cutoff value to be −584 HU.

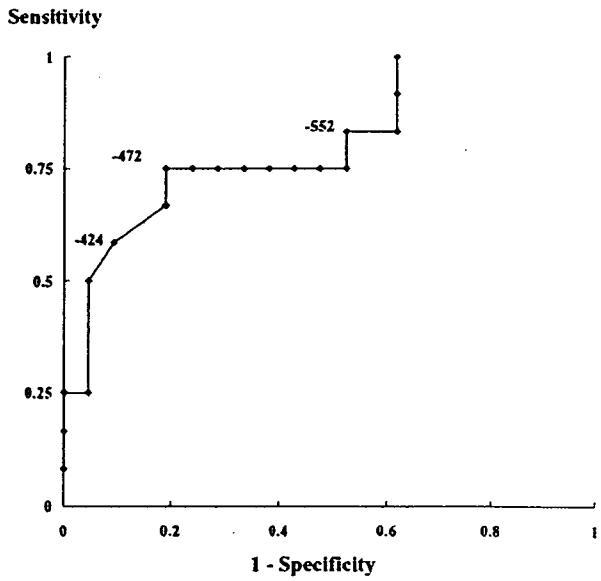

FIGURE 4. ROC curve of the mean CT number for differentiation between BAC and adenocarcinoma, showing the cutoff value to be −472 HU.

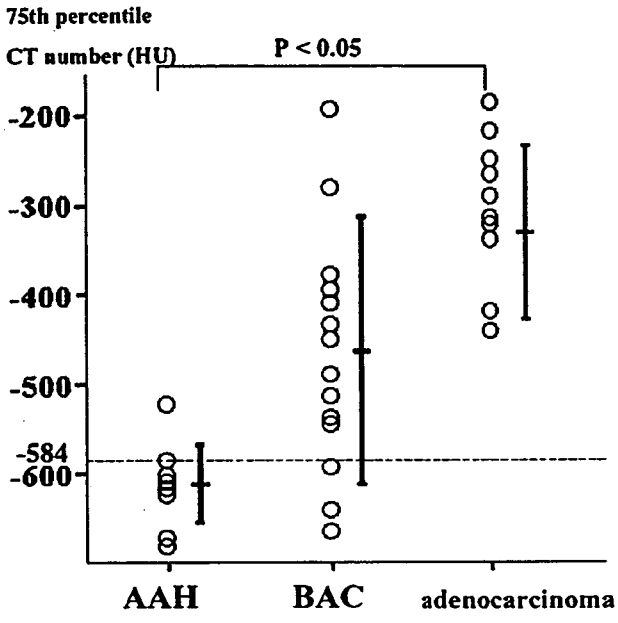

FIGURE 5. The plots of the CT number of the 75th percentile in AAH, BAC, and adenocarcinoma lesions. The dotted line indicates a −584-HU cutoff value between AAH and BAC. The differences between AAH and BAC, and between BAC and adenocarcinoma were significant ($p < 0.05$). Bars = mean ± SD.

BAC lesions could not be distinguished from each other by the 75th percentile CT number. Histologic findings of one indistinguishable AAH lesion showed

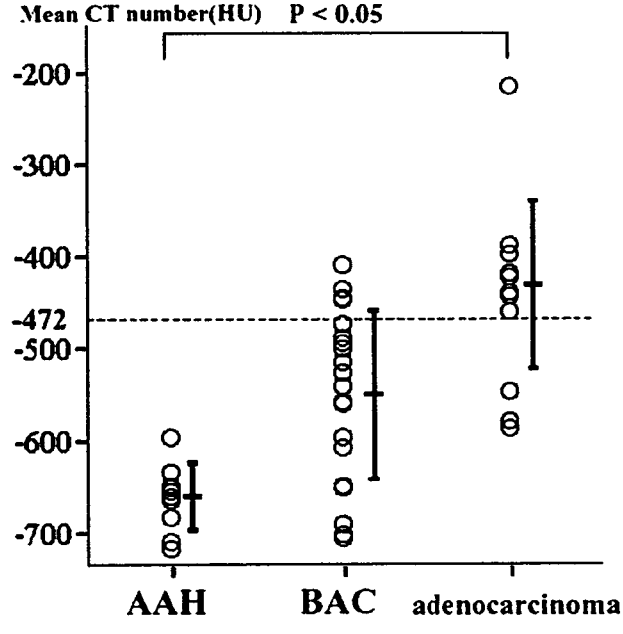

FIGURE 6. The plots of the mean CT number in AAH, BAC, and adenocarcinoma. The dotted line indicates a −472-HU cutoff value between BAC and adenocarcinoma. The differences between AAH and BAC, and between BAC and adenocarcinoma were significant ($p < 0.01$). Bars = mean ± SD.

Table 4—*Differentiation Between AAH and BAC With the 75th Percentile CT Number

75th Percentile CT No.	AAH	BAC	Total
≤ −584 HU	9	5	14
> −584 HU	1	16	17
Total	10	21	31

*Data are presented as No.

reasonable cellularity and nuclear atypia as typically seen in AAH, but had thickened alveolar septa like BAC, resulting in a higher 75th percentile value than the cutoff value. Five indistinguishable BAC lesions showed reasonable nuclear atypia as typically seen in BAC, but they had less thickened alveolar septa than usually seen in BAC, resulting in lower 75th percentile values than the cutoff value. It is well known that histologic differentiation between AAH and BAC is sometimes difficult. Kitamura et al classified AAH lesions into low grade and high grade, of which the later was histologically similar to BAC.[15] Therefore, we consider that the complete differentiation between AAH and BAC is difficult even using the 3D analysis of CT number. However, this study showed that all of the 10 AAH lesions showed one peak on the CT number histogram, whereas 38% of BAC lesions and 42% of adenocarcinoma lesions showed two peaks. It is also well known that AAH lesions usually appear as pure GGOs, whereas some BAC and adenocarcinoma lesions appear as GGOs mixed with a solid component. The CT number histogram pattern can clearly reveal a mixed solid component within GGO lesions as the second peak; therefore, AAH can be ruled out and recommended for surgical resection when the histogram shows a two-peak pattern.

In contrast, the CT number histogram pattern (*ie*, one or two peaks) could not be used to differentiate between BAC and adenocarcinoma. While the peak at the high CT number zone on the histogram in cases of adenocarcinoma usually showed an increased amount of central fibrosis, that in BAC showed an area of alveolar structural collapse, both of which can be easily distinguished from pathologic findings.[16] However, HRCT imaging has a very

Table 5—*Differentiation Between Adenocarcinoma and BAC With the Mean CT Numbers

Mean CT No.	BAC	Adenocarcinoma	Total
≤ −472	17	3	20
> −472	4	9	13
Total	21	12	33

*Data are presented as No.

limited ability to distinguish between tumor fibrosis and alveolar structural collapse, resulting in a similar frequency of two peak patterns between BAC and adenocarcinoma. In contrast, the lesions with higher than −472 HU of mean CT numbers were more frequently adenocarcinoma than BAC. Therefore, mean CT number is more useful in differentiating between BAC and adenocarcinoma.

While a BAC lesion of < 2 cm has been reported[17,18] to be able to be cured by wedge resection, adenocarcinoma should be treated by lobectomy or segmentectomy even for stage p-T1N0M0 disease, because a wedge resection can cause a local relapse due to the spread of tumor cells into lymphatic vessels outside the primary tumor.[19] We believe that mean CT number could determine operative procedures for GGO lesions.

How often and how long do the GGO lesions suspected of AAH need to be followed by CT scanning? By analogy with multistep carcinogenesis, AAH could progress to adenocarcinoma through BAC. Even if AAH subsequently develops into BAC, follow-up with CT scanning would not miss the chance of surgical cure, because the lesion would remain within the T1N0M0 stage during the follow-up period until it grows to a diameter of 2 cm.[2,16] Aoki et al[3] reported that the mean tumor doubling time of BAC was 880 days. Therefore, careful follow-up by CT scanning every 2 years would be enough for GGO lesions suspected to be AAH.

We conclude the following from the 3D analysis of the CT number of GGO lesions: (1) two peaks on the CT number histogram can rule out AAH; (2) the 75th percentile is the optimal CT number for differentiating between AAH and BAC; and (3) the mean CT number is the optimal CT number to differentiate between BAC and adenocarcinoma. While it has been time-consuming to obtain information on 3D imaging from CT scans, we believe that further advances in software and CAD systems will make the procedure reported in this study easier.

References

1 Kuriyama K, Seto M, Kasugai T, et al. Ground-glass opacity on thin-section CT: value in differentiating subtypes of adenocarcinoma of the lung. AJR Am J Roentgenol 1999; 173:465–469

2 Higashiyama M, Kodama K, Yokouchi H, et al. Prognostic value of bronchiolo-alveolar carcinoma component of small lung adenocarcinoma. Ann Thorac Surg 1999; 68:2069–2073

3 Aoki T, Nakata H, Watanabe H, et al. Evolution of peripheral lung adenocarcinomas: CT findings correlated with histology and tumor doubling time. AJR Am J Roentgenol 2000; 174:763–768

4 Kodama K, Higashiyama M, Yokouchi H, et al. Prognostic value of ground-glass opacity found in small lung adenocarcinoma on high-resolution CT scanning. Lung Cancer 2001; 33:17–25

5 Nomori H, Ohtsuka T, Naruke T, et al. Differentiating between atypical adenomatous hyperplasia and bronchioloalveolar carcinoma using the computed tomography number histogram. Ann Thorac Surg 2003; 76:867–871

6 Nomori H, Ohtsuka T, Naruke T, et al. Histogram analysis of computed tomography numbers of clinical T1N0M0 lung adenocarcinoma with special reference to lymph node metastasis and tumor invasiveness. J Thorac Cardiovasc Surg 2003; 126:1584–1589

7 Matsuguma H, Nakahara R, Anraku M, et al. Objective definition and measurement method of ground-glass opacity for planning limited resection in patients with clinical IA adenocarcinoma of the lung. Lung Cancer 2004; 25:1102–1106

8 Nakata M, Sawada S, Yamashita M, et al. Objective radiological analysis of ground-glass opacity aimed at curative limited resection for small peripheral non-small cell lung cancer. J Thorac Cardiovasc Surg 2005; 129:1226–1231

9 Travis MD, Colby TV, Corrin B, et al. World Health Organization international histological classification of tumors: histological typing of lung and pleural tumors. 3rd ed. Berlin, Germany: Springer-Verlag, 1999

10 Brambilla E, Travis WD, Colby TV, et al. The new World Health Organization classification of lung tumors. Eur Respir J 2002; 18:1059–1068

11 Awai K, Murao K, Ozawa A, et al. Pulmonary nodules at chest CT: effect of computer-aided diagnosis on radiologists detection performance. Radiology 2004; 230:347–352

12 Awai K, Murao K, Ozawa A, et al. Pulmonary nodules: estimation of malignancy at thin-section helical CT-effect of computer-aided diagnosis on performance of radiologists. Radiology 2006; 239:276–284

13 Kass M, Witkin A, Terzopoulos D. Snakes: active contour models. Int J Comput Vis 1988; 1:321–331

14 Dougherty E. Digital image processing method. In: Thompson BJ, ed. Optical engineering. New York, NY: Dekker, 1994; 77–85

15 Kitamura H, Kameda Y, Nakamura N, et al. Proliferative potential and p53 overexpression in precursor and early stage lesions of bronchioloalveolar lung carcinoma. Am J Pathol 1995; 146:876–887

16 Noguchi M, Morikawa A, Kawasaki M, et al. Small adenocarcinoma of the lung: histologic characteristics and prognosis. Cancer 1995; 75:2844–2852

17 Nakata M, Sawada S, Saeki H, et al. Prospective study of thoracoscopic limited resection for ground-glass opacity selected by computed tomography. Ann Thorac Surg 2003; 75:1601–1606

18 Yoshida J, Nagai K, Yokose T, et al. Limited resection trial for pulmonary ground-glass opacity nodules: fifty-case experience. J Thorac Cardiovasc Surg 2005; 129:991–996

19 Ichinose Y, Yano T, Yokoyama H, et al. The correlation between tumor size and lymphatic vessel invasion in resected peripheral stage I non-small cell lung cancer: a potential risk of limited resection. J Thorac Cardiovasc Surg 1994; 108: 684–686

Case Report

Treatment of a Fractured Ultraflex Stent Causing Tracheal Stenosis

Takeshi Mori, MD, Hiroaki Nomori, MD, PhD, Masakazu Yoshioka, MD, Hironori Kobayashi, MD, Kazunori Iwatani, MD, and Koei Ikeda, MD, PhD

We report on a case of a fractured Ultraflex stent after placement for malignant tracheal stenosis. The patient was a 49-year-old female with adenoid cystic carcinoma of the trachea causing airway stenosis. She was treated by non-covered Ultraflex stent followed by chemoradiotherapy. Twenty months after stent placement, more than half of the distal end of the stent was fractured and caused airway stenosis, while there was no tumor regrowth. After dilation by balloon and bougienage using an endotracheal tube, an additional non-covered Ultraflex stent was placed within the first one, resulting in successful dilation. The patient is now well without any problem with the stent, 12 months after the second stent placement. (Ann Thorac Cardiovasc Surg 2007; 13: 195–197)

Key words: stent, Ultraflex, tracheal stenosis, balloon, bougienage

Introduction

The Ultraflex stent has been widely used for stenosis not only the tracheobronchus but also the digestive tract, e.g., the esophagus and colon.[1,2] While there have been several reported cases in which the Gianturco type expandable metallic stent has fractured and caused airway stenosis,[3] no fractures of the Ultraflex stent has been reported. We report a case with tracheal stenosis due to a fractured wire of an Ultraflex stent after placement for tracheal adenoid cystic carcinoma. We also present a treatment method for the problem and its outcome. As far as we know, this is the first reported case and treatment of this problem.

Case Report

A 49-year-old female patient was complaining of a dry cough and dyspnea on exertion in July 2003. Computed tomography (CT) revealed tracheal stenosis, and she was referred to our hospital. Brochoscopy demonstrated stenosis of the lower trachea by tumor (Fig. 1), which was diagnosed as an adenoid cystic carcinoma on biopsy. As the tumor had spread to almost the entire length of the intrathoracic trachea, the patient was treated by stent placement followed by chemoradiotherapy. On August 19, 2003, a non-covered Ultraflex stent (Boston Scientific Co., Natick, MA) 18 mm in diameter and 60 mm in length was placed at the stenotic site. This resulted in a sufficient dilation of the stenosis and improvement in her symptoms. After chemoradiotherapy, CT and bronchoscopy revealed a significant decrease of the tumor. However, in January 2005, she began to complain of dyspnea and wheezing, which had been gradually worsening. In July 2005, CT and bronchoscopy revealed that over than half the distal stent had fractured, resulting in projection of the fractured wire into the tracheal lumen, causing tracheal stenosis (Fig. 2). No tumor regrowth was observed on CT and bronchoscopy. Because the fractured wire projecting into the lumen might interfere with an additional Ultraflex stent, causing insufficient dilation, the balloon dilation by means of a cuff of the endotracheal tube was performed for 15 min, which did not expand the fractured wire. Therefore, a continuous balloon dilation and bougienage method was performed before an additional

From Department of Thoracic Surgery, Graduate School of Medical Sciences, Kumamoto University, Kumamoto, Japan

Received August 28, 2006; accepted for publication October 23, 2006

Address reprint requests to Hiroaki Nomori, MD, PhD: Department of Thoracic Surgery, Graduate School of Medical Sciences, Kumamoto University, 1–1–1 Honjo, Kumamoto 860–8556, Japan.

Fig. 1. Bronchoscopy showed growth of tracheal tumor, causing tracheal stenosis before first stenting.

Fig. 2. Bronchoscopy showed that a fractured wire was projected into the lumen, causing tracheal stenosis.

stent placement.

After tracheostomy, an endotracheal tube 9 mm in internal diameter (ID) was introduced. The cuff of the tube was inflated with air at the stenotic site, and the tube was fixed at the tracheostomy (Fig. 3). After two days, the endotracheal tube was changed to a larger one (10 mm in ID), on which the cuff was also dilated at the stenotic site. This balloon dilation and bougienage was continued for five days in total. After five days, the fractured wire projected into the tracheal lumen which had become pressed toward the tracheal wall (Fig. 4). An additional non-covered Ultraflex stent of the same size was placed within the same site of the first one, resulting in sufficient dilation of the trachea (Fig. 5). After the stent placement, the patient's symptoms disappeared. She remains well without any problem with the stent twelve months after the second stent placement.

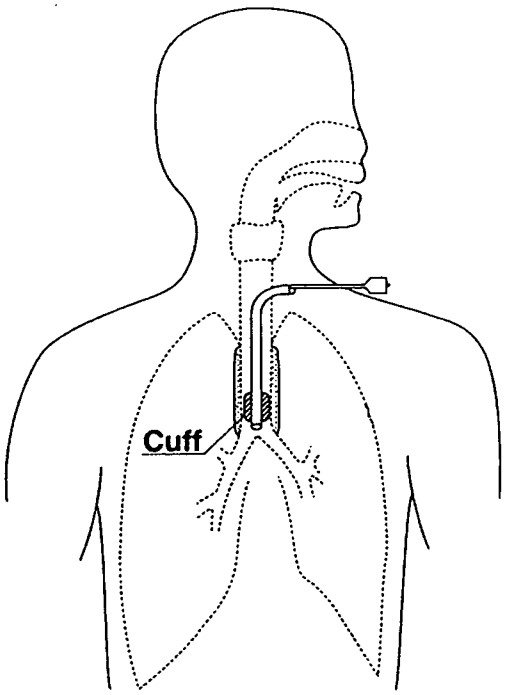

Fig. 3. Schema of continuous balloon dilation and bougienage by using endotracheal tube via tracheostomy tube.

Discussion

As an Ultraflex stent is usually not removable after long term placement, a fractured stent causing airway stenosis needs an additional stent placement. While an Ultraflex stent and Dumon stent are both options, we recommend the former, because the Dumon stent could impede sputum drainage by complete blockade of ciliary movement, especially when a long stent is used.[4] However, before placement of an additional Ultraflex stent within the fractured one, it was necessary to press the fractured wire toward the tracheal wall because it could catch on the additional stent and block sufficient expansion. There-

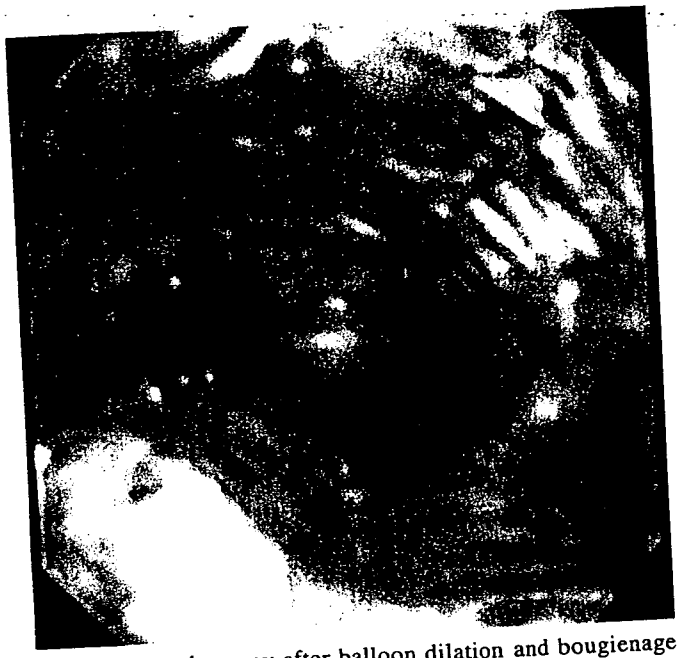

Fig. 4. Bronchoscopy after balloon dilation and bougienage showed that a projected wire was completely pressed to the tracheal wall.

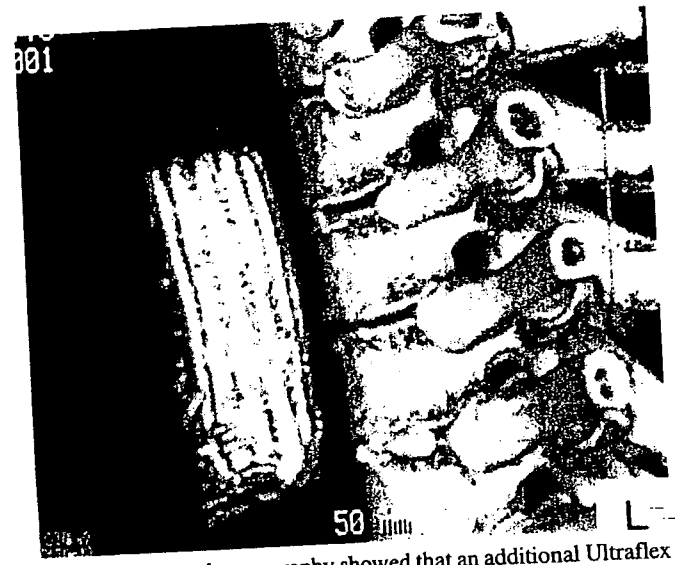

Fig. 5. Computed tomography showed that an additional Ultraflex stent sufficiently maintained the dilation of trachea.

fore, the balloon dilation and bougienage using an endotracheal tube via tracheostomy were performed for a few days, as previously reported,[5] which resulted in sufficient dilation of stenotic wire to enable additional stent placement. We believe this dilation method is not only effective but also safe, and should be carried out before additional stent placement for a fractured stent causing airway stenosis.

References

1. Madden BP, Datta S, Charokopos N. Experience with Ultraflex expandable metallic stents in the management of endobronchial pathology. *Ann Thorac Surg* 2002; **73**: 938–44.
2. De Palma GD, Galloro G, Sivero L, et al. Self-expanding metal stents for palliation of inoperable carcinoma of the esophagus and gastroesophageal junction. *Am J Gastroenterol* 1995; **90**: 2130–2.
3. Heinrich DB. Stenting of central airways. *J Bronchol* 1995; **2**: 98–106.
4. Nomori H, Kobayashi R, Kodera K, Morinaga S, Ogawa K. Indications for an expandable metallic stent for tracheobronchial stenosis. *Ann Thorac Surg* 1993; **56**: 1324–8.
5. Nomori H, Horio H, Suemasu K. Bougienage and balloon dilation using a conventional tracheal tube for tracheobronchial stenosis before stent placement. *Surg Endosc* 2000; **14**: 587–91.

Sentinel node identification in clinical stage Ia non–small cell lung cancer by a combined single photon emission computed tomography/computed tomography system

Hiroaki Nomori, MD, PhD,[a] Koei Ikeda, MD, PhD,[a] Takeshi Mori, MD, PhD,[a] Shinya Shiraishi, MD, PhD,[b] Hironori Kobayashi, MD,[a] Kazunori Iwatani, MD,[a] Koichi Kawanaka, MD, PhD,[b] and Toshiaki Kobayashi, MD, PhD[c]

Drs Nomori, Mori, and Ikeda (*left to right*). The bronze statue is Dr. Shibasaburo Kitasato.

Objective: A gamma probe can identify sentinel nodes before nodal dissection in the mediastinum but not in the hilum, owing to high radioactivity from primary tumors. We evaluated the utility of fused single photon emission computed tomography/computed tomography (SPECT/CT) images for the identification of sentinel nodes in the hilum for patients with clinical stage Ia non–small cell lung cancer.

Methods: Technetium-99m tin colloid was injected into the peritumoral region approximately 18 hours before surgery in 63 patients with clinical stage Ia non–small cell lung cancer. On the morning of the operation, approximately 16 hours after administration of tin colloid, sentinel nodes were identified by fused SPECT/CT; this was followed by intraoperative sentinel node identification in the dissected lymph nodes by gamma probe. Because the gamma probe is a standard method for sentinel node identification, the sensitivity of fused SPECT/CT images was examined on the basis of the data of the gamma probe.

Results: Fused SPECT/CT images could identify sentinel nodes at segmental and lobar lymph nodes with a sensitivity of 0.87 and 0.74, both of which were significantly higher than 0.40 in the mediastinum ($P < .001$ and $P = .012$, respectively). In 5 patients with pathologic N1 or N2 disease, both SPECT/CT and the gamma probe could identify sentinel nodes with metastases.

Conclusions: SPECT/CT could identify sentinel nodes of the hilum especially in segmental and lobar lymph nodes but not in the mediastinum. Because the gamma probe can identify sentinel nodes before nodal dissection in the mediastinum but not in the hilum, a combination of SPECT/CT and the gamma probe can be used to identify sentinel nodes before nodal dissection in both the hilum and the mediastinum, which will enable sentinel node navigation surgery in non–small cell lung cancer.

From the Departments of Thoracic Surgery[a] and Radiology,[b] Graduate School of Medical Sciences, Kumamoto University, Honjo, Kumamoto, and the [c]Department of Assistive Diagnostic Technology, National Cancer Center Hospital, Tsukiji, Chuo-ku, Tokyo, Japan.

Received for publication Dec 3, 2006; revisions received Jan 21, 2007; accepted for publication Feb 7, 2007.

Address for reprints: Hiroaki Nomori, MD, PhD, Department of Thoracic Surgery, Graduate School of Medical Sciences, Kumamoto University, 1-1-1 Honjo, Kumamoto 860-8556, Japan (E-mail: hnomori@qk9.so-net.ne.jp).

J Thorac Cardiovasc Surg 2007;134:182-7

0022-5223/$32.00

doi:10.1016/j.jtcvs.2007.02.013

GTS

Sentinel lymph node (SN) sampling with a gamma probe has allowed surgeons to be more selective in performing a formal lymph node dissection in melanoma, breast cancer, and gastrointestinal cancers.[1-3] However, the gamma probe method in lung cancer surgery cannot identify SNs before lymph node dissection in the hilum owing to high radioactivity from primary tumors.[4,5] Therefore, previously reported SN identifications with the gamma probe method in lung cancer surgery have been based on radioactivity measured in the dissected lymph nodes,[5-10] which cannot be used to guide lymph node dissection or sampling. This difficulty with the gamma probe method makes it difficult for SN navigation surgery to be of practical use in non–small cell lung cancer (NSCLC).

Planar scintigram with a radioactive colloid has also been used to identify SNs, especially in melanoma of the head and neck.[11-13] However, in lung cancer surgery, localization of nodal stations by planar scintigram is difficult because SNs cannot

Abbreviations and Acronyms
CT = computed tomography
NSCLC = non–small cell lung cancer
SN = sentinel lymph node
SPECT = single photon emission computed tomography
^{99m}Tc = technetium-99m

readily be discriminated owing to the lack of tomography images. In 2002, we installed a combined single photon emission computed tomography/computed tomography (SPECT/CT) system that is composed of a gantry-free gamma camera and an 8-row multidetector CT. So that we can avoid positional differences between the SPECT and CT studies, imaging is performed on the same platform, which makes fusion of SPECT and high-performance CT images possible. Because the SPECT/CT system has enabled us to identify SNs on the basis of the fusion images, without the adverse effect of overlapping radioactivity from the primary site, it allows preoperative SN localization in relation to nearby anatomic structures, which enables an intraoperative SN biopsy to be easy and accurate. We[14] previously identified SNs in 35 patients with melanoma by the SPECT/CT system; the identification rate was 100%.[14] The present study evaluated the usefulness of fused SPECT/CT images, compared with the gamma probe, for SN identification in lung cancer surgery.

Patients and Methods

Patient Eligibility

This study of SN identification in patients with clinical stage Ia NSCLC was approved by the ethical committee of the Graduate School of Medical Sciences, Kumamoto University, in March 2005. Clinical staging was performed by body CT, brain magnetic resonance imaging, and positron emission tomography. Informed consent was obtained from all patients after a discussion with the surgeons regarding the risks and benefits. Eligible patients had clinical stage Ia peripheral type NSCLC and were candidates for lobectomy or segmentectomy with mediastinal lymph node dissection. The patients without preoperative histologic diagnosis of tumors were excluded. The lobectomy with mediastinal lymph node dissection was performed via thoracoscopy, as described before.[15] Segmentectomy with hilar and mediastinal lymph node dissection was performed via open thoracotomy, as described before.[16] All of the lymph nodes at the hilum were dissected during segmentectomy with taping of the vessels and bronchus.

Lymph Node Nomenclature

The lymph node nomenclature used was based on the original lymph node map for lung cancer.[17]

Administration of Radioactive Colloid

Administration of the radioactive colloid was based on the method reported previously.[4,5] In the SPECT/CT room, approximately 18 hours before the operation, 6 to 8 mCi of technetium-99m (^{99m}Tc) tin colloid suspended in a volume of 1 to 1.5 mL was injected into the peritumoral region.

SPECT/CT System

On the morning of the operation, approximately 16 hours after administration of the ^{99m}Tc tin colloid, SNs were identified by the SPECT/CT system. This system was composed of a commercially available gantry-free SPECT with dual-head detectors (Skylight; ADAC Laboratories, Milpitas, Calif) and an 8 multidetector-row CT scanner (Light-Speed Ultra Instrument; General Electric, Milwaukee, Wis). The two instruments were juxtaposed so that the CT table bearing the patient could be moved directly into the SPECT scanner before CT scanning. As a result, each patient was identically positioned for SPECT and CT imaging.

SPECT data acquisition was performed with a vertex general-purpose parallel-hole (VXGP) collimator. A 360 SPECT scan was acquired and was followed by CT scanning. Reconstructive CT images were processed into Digital Imaging and Communications in Medicine (DICOM) data and then transferred to Pegasys (ADAC Laboratories, Milpitas, Calif), which is a workstation for SPECT processing. One lumen of a 3-way stopcock (inner diameter 4 mm, length 10 mm) containing an aqueous solution of ^{99m}Tc tin colloid and a contrast medium was used as an external fiducial marker. So that a precise record of both images could be obtained, external fiducial markers were fixed to the common platform for SPECT and CT imaging. The two scans were performed sequentially. Fusion of the SPECT images with the CT images was manually performed by aligning the external fiducial markers of the two images on the workstation, enabling localization of SN on CT images (Figure 1). An SN was visually identified on the SPECT/CT images by two experienced radiologists before surgery (S.S. and K.K).

Gamma Probe Method

The radioactivity of the dissected lymph nodes was determined by a handheld gamma probe (Navigator; Auto Suture Japan, Tokyo, Japan), as reported previously.[4,5] An SN was defined as any node for which the radioactivity count was 10 times that of the background level.

Pathologic Examination

SNs were examined by intraoperative frozen section analysis using 2- to 3-mm thick sections. The dissected lymph nodes were examined histologically by use of formalin-fixed and paraffin-embedded sections with hematoxylin and eosin staining.

Statistical Analysis

Because the use of a gamma probe to measure radioactivity of dissected lymph nodes is now a standard method for SN identification, the sensitivity of SPECT/CT was examined on the basis of data gathered with the gamma probe, which was calculated as true positive/true positive + false negative. All data were analyzed for statistical significance by the χ^2 test. All values in the text and tables are given as mean ± standard deviation.

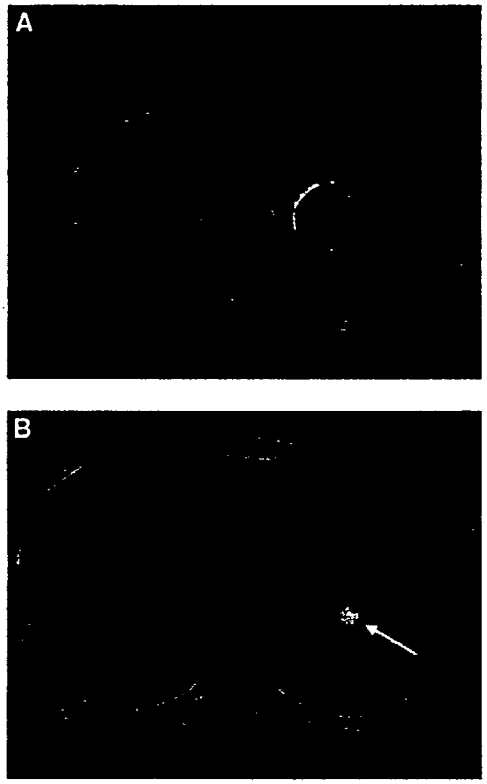

Figure 1. Fused SPECT/CT images in lung cancer of the left upper lobe. A, Primary tumor. B, Radiolabeled lymph node (segmental nodal station) can be detected *(arrow)*.

TABLE 1. Patient characteristics of SN identification by gamma probe

	Sentinel nodes by gamma probe	
	Identified	Not identified
Age (y)		
Mean ± SD	68 ± 7	74 ± 8*
Range	53-81	65-82
Sex (No.)		
Male	25	10
Female	24	4
Mean tumor size (mm)	19 ± 7	24 ± 8†
Tumor location (No.)		
Right upper lobe	13	3
Right middle lobe	2	1
Right lower lobe	8	3
Left upper lobe	17	5
Left lower lobe	9	2
Histologic type (No.)		
Adenocarcinoma	44	8
Squamous cell carcinoma	3	6
Adenosquamous carcinoma	1	0
Small cell carcinoma	1	0
Operative procedure (No.)		
Lobectomy	7	4
Segmentectomy	42	10
p-TNM (No.)		
T1 N0 M0	43	13
T2 N0 M0	1	1
T1 N1 M0	2	0
T1 N2 M0	3	0
Total	49	14

SN, Sentinel node. *P = .01; †P = .024.

Results

From April 2005 to September 2006, 79 patients with clinical stage Ia peripheral NSCLC underwent surgery at the Department of Thoracic Surgery of Kumamoto University Hospital. Of these, 16 patients could not be enrolled in this study because of the following reasons: (1) Preoperative histologic diagnosis was not obtained in 5 patients; (2) SPECT/CT could not be used because of the other examinations in 10 patients; and (3) one patient refused to participate in the study. As a result, 63 consecutive patients were enrolled in this study. The gamma probe identified SNs in 49 (78%) of the 63 patients, whose pathologic N stages were N0 in 44, N1 in 2, and N2 in 3 (Table 1). SPECT/CT could identify SNs in 39 (62%) patients, whose pathologic N stages were N0 in 34, N1 in 2, and N2 in 3 (Table 2). The SN identification rate by SPECT/CT imaging was lower than that achieved by the gamma probe with marginal significance (P = .052). The mean number of SNs identified by the gamma probe in the 48 patients was 1.6 ± 0.8 (range: 1-4); the value obtained by SPECT/CT in the 38 patients was 1.5 ± 0.6 (range: 1-3). However, there was no significant difference between the two methods in this respect. Between the 49 patients with identifiable SNs and the 14 without by gamma probe, the mean age was younger and the mean tumor size was smaller in the former than in the latter, with significance (P = .01 and .024, respectively). However, there were no significant differences of other variables between patients with identifiable SNs and those without when both the gamma probe and SPECT/CT were used. Tumors in 2 patients were pathologically classified as T2: one tumor was involved over the pleura and the other one was larger than 3 cm in the permanent section. Although 2 patients needed tube drainage because of pneumothorax after the injection of the isotope, there were no other complications.

Table 3 shows the correlation between SPECT/CT imaging and the gamma probe method for SN identification at each nodal station of the hilum and mediastinum in the 49 patients whose SNs were identified by gamma probe. In the lymph node stations at the hilum, the gamma probe and SPECT/CT corresponded with each other in 46 (94%) patients at nodal station No. 10, 46 (94%) at No. 11, 42 (86%)

GTS

at No. 12, and 39 (80%) at No. 13. In the mediastinum of the right lung, the gamma probe and SPECT/CT corresponded with each other in 21 (91%) patients at nodal station No. 3, in 22 (96%) at No. 4, and in 22 (91%) at No. 7. In the mediastinum of the left lung, the gamma probe and SPECT/CT corresponded with each other in 26 (100%) patients at nodal station No. 4, in 22 (85%) at No. 5, and in 22 (85%) at No. 7. SNs were not identified at the other mediastinal nodal stations, that is, Nos. 1, 2, 8, and 9, using both methods.

The sensitivity of SPECT/CT based on Table 3 was 0.82 at nodal station No. 13, 0.74 at No. 12, 0.63 at No. 11, 0.40 at No. 10, and 0.31 at the mediastinal nodal stations (Figure 2). The sensitivity of SPECT/CT decreased numerically from nodal station No. 13 to No. 10 and was the lowest in the mediastinal lymph nodes. The sensitivity of SPECT/CT in the mediastinal lymph nodes was significantly lower than those at nodal station No. 13 and No. 12 ($P < .001$ and $P = .012$, respectively). The specificity of SPECT/CT based on Table 3 was 0.76 at No. 13, 0.93 at N0. 12, 1.0 at N0. 11, 1.0 at No. 10, and 0.99 at the mediastinum.

TABLE 2. Patient characteristics of SN identification by SPECT/CT

	SNs by SPECT/CT	
	Identified	Not identified
Age (y)		
Mean ± SD	68 ± 6	69 ± 7
Range	54-81	53-82
Sex (No.)		
Male	20	15
Female	19	9
Mean tumor size (mm)	19 ± 7	20 ± 7
Tumor location (No.)		
Right upper lobe	11	5
Right middle lobe	0	3
Right lower lobe	7	4
Left upper lobe	15	7
Left lower lobe	6	5
Histologic type (No.)		
Adenocarcinoma	34	18
Squamous cell carcinoma	4	5
Adenosquamous carcinoma	0	1
Small cell carcinoma	1	0
Operative procedure (No.)		
Lobectomy	5	6
Segmentectomy	34	18
pTNM (No.)		
T1 N0 M0	33	23
T2 N0 M0	1	1
T1 N1 M0	2	0
T1 N2 M0	3	0
Total	39	24

SN, Sentinel node; *SPECT/CT*, single photon emission computed tomography.

TABLE 3. Correlation between SPECT/CT and gamma probe for SN identification

	Patient number with SN identified by				
	Gamma probe (+)		Gamma probe (−)		
Station	SPECT (+) True positive	SPECT (−) False negative	SPECT (+) False positive	SPECT (−) True negative	Total
Hilum					
10	2	3	0	44	49
11	5	3	0	41	49
12	14	5	2	28	49
13	23	5	5	16	49
Mediastinum					
Right					
3	1	2	0	20	23
4	1	1	0	21	23
7	0	1	0	22	23
Left					
4	1	0	0	25	26
5	2	3	1	20	26
7	0	4	0	22	26

SN, Sentinel node; *SPECT/CT*, single photon emission computed tomography. +, Sentinel node is identified; −, sentinel node is not identified.

Pathologic examination showed lymph node metastases in 5 patients, that is, N1 in 2 patients and N2 in 3 (Table 4). Frozen section of the SNs identified by both SPECT/CT and the gamma probe could show metastases in all 5 patients.

Discussion

The present study demonstrated that SPECT/CT was inferior to the gamma probe method for SN identification in the mediastinal lymph nodes. This discrepancy could be caused by the following: (1) the ability to measure radioactivity with SPECT/CT images is inferior to that of direct mea-

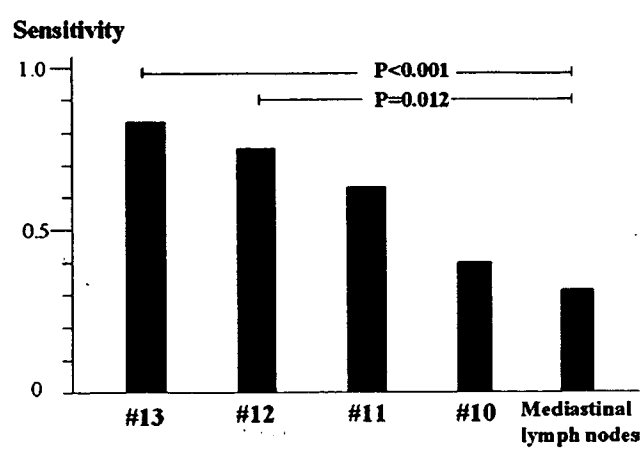

Figure 2. Sensitivity of SPECT/CT at each lymph node station.

TABLE 4. SNs identified by SPECT/CT and gamma probe in patients with N1 or N2 disease

No.	Age/sex	Tumor location	Histology	Metastatic node	SN		pTNM
					SPECT/CT	Gamma probe	
1	60/M	RLL	Ad	No. 13	No. 13	No. 13	T1 N1 M0
2	72/M	RLL	Ad	No. 11	No. 11	No. 11	T1 N1 M0
3	80/M	LUL	Ad	No. 5	No. 5	No. 5	T1 N2 M0
4	59/M	LUL	Ad	Nos. 5, 12, 13	Nos. 12, 13	Nos. 5, 12	T1 N2 M0
5	54/F	LLL	Ad	Nos. 7, 11, 12	Nos. 12, 13	No. 12	T1 N2 M0

SPECT/CT, Single photon emission computed tomography/computed tomography; *RLL*, right lower lobe; *LUL*, left upper lobe; *LLL*, left lower lobe; *Ad*, adenocarcinoma.

surement by a gamma probe and (2) the radioactivity of mediastinal SNs is usually lower than that of hilar SNs, because the former is further away from the primary tumor. Therefore, we conclude that SPECT/CT cannot easily identify SNs in the mediastinum. However, SPECT/CT could identify SNs at nodal station No. 12 and No. 13 with a sensitivity of 0.82 and 0.74, respectively. This may be because SNs at nodal station No. 12 and No. 13 are close to the primary tumor, which makes their radioactivity high enough for detection by SPECT/CT. In fact, in 5 patients with N1 or N2 disease, SPECT/CT imaged metastatic SNs in the hilum before the operation.

We[4] previously evaluated SN identification by using a gamma probe in 104 patients with clinical stage I NSCLC and concluded that although the gamma probe could identify SNs in the mediastinum before lymph node dissection (in vivo SN identification), it could not in the hilum owing to high radioactivity from primary tumors. Because the present study showed the usefulness of SPECT/CT for the in vivo SN identification in the hilum, we believe that the combination of SPECT/CT and the gamma probe could be useful for in vivo SN identification in both the hilum and the mediastinum.

Recently, it has been reported that segmentectomy could be an alternative to lobectomy for pathologic T1 N0 M0 NSCLC.[16,18,19] So that the final indication of segmentectomy can be determined, intraoperative frozen sections must be examined for all of the hilar and lobe-specific mediastinal lymph nodes to confirm the intraoperative N stage to be N0.[18,19] We consider that the application of SPECT/CT could be used for determining the final indication of segmentectomy as follows: (1) SNs identified in the hilum by SPECT/CT and those identified in the mediastinum by gamma probe are submitted for frozen sections; (2) when frozen sections of SNs show metastases, segmentectomy is converted to lobectomy. Even after segmentectomy, in vivo SN identification by gamma probe is usually difficult for the hilum owing to high radioactivity in the remaining segments. Therefore, if SPECT/CT is not used, all lymph nodes in the hilum have to be dissected during segmentectomy for SN identification by gamma probe, which is hard as well as time-consuming. On the other hand, for lobectomy, SN identification by SPECT/CT would not be necessary because lymph nodes at the hilum are routinely removed during lobectomy and can be examined for SN identification by gamma probe.

The sensitivities of SN identification at nodal station No. 10 and No. 11 by SPECT/CT were still low. Because station No. 10 is close to the mediastinum, the gamma probe can identify SNs at this station after resection of the primary tumor, as there will no longer be any interference of radioactivity from the primary tumor. Nodal station No. 11 is usually easy to excise even during segmentectomy, enabling SN identification by gamma probe.

Several tracers have been used for SN identification, such as ^{99m}Tc tin colloid, ^{99m}Tc sulfur colloid, and ^{99m}Tc phytate. Of these, ^{99m}Tc tin colloid has the largest particles, that is, about 1000 nm in diameter. The reason that we have used ^{99m}Tc tin colloid is as follows. Because the particles of tin colloid are large, they take longer to reach SNs than the other tracers with small particles. In lung cancer surgery, unlike operations for cancer in other organs, radioisotope injected frequently leaks into the tracheobronchus, which makes in vivo SN identification unreliable immediately after the injection. Because ^{99m}Tc tin colloid has to be injected a few hours before the operation to reach SNs, the material that leaked into the tracheobronchus is already washed out at surgery, resulting in more reliable in vivo SN identification than the other tracers with small particles.[4] We[4] previously confirmed that the radioactivity of ^{99m}Tc tin colloid in SNs was stable from 9 to 24 hours after the injection. On the other hand, ^{99m}Tc sulfur colloid can reach SNs rapidly because of their small particles, approximately 40 nm in diameter, but could pass through the true SNs and flow further up the chain of nodes, resulting in false negative results. Therefore, ^{99m}Tc sulfur colloid has to be injected immediately before surgery, which would make the in vivo SN identification difficult because of material leaking into the tracheobronchus. In fact, the previous reports using ^{99m}Tc sulfur colloid identified SNs in the dissected lymph nodes but not with in vivo identification.[6,7]

In conclusion, SPECT/CT can be used to identify SNs in the hilum before surgery, especially at nodal station No. 12 and No. 13, but not in the mediastinum. Because the gamma probe method can identify SN before lymph node dissection in the mediastinum but not in the hilum, a combination of SPECT/CT and the gamma probe could be used to identify SNs before lymph node dissection in both the hilum and the mediastinum. This will enable SN navigation surgery in patients with clinical stage Ia NSCLC, especially for segmentectomy.

References

1. Tafra L, Lannin DR, Swanson MS, Eyk JJV, Verbanac KM, Chua AN, et al. Multicenter trial of sentinel node biopsy for breast cancer using both technetium sulfur colloid and isosulfan blue dye. *Ann Surg.* 2001; 233:51-9.
2. Morton DL, Thompson JF, Essner R, Elashoff R, Stern SL, Nieweg OE, et al. Validation of the accuracy of intraoperative lymphatic mapping and sentinel lymphadenectomy for early-stage melanoma. *Ann Surg.* 1999;230:453-65.
3. Kitagawa Y, Fujii H, Mukai M, Kubota T, Ando N, Watanage M, et al. The role of the sentinel lymph node in gastrointestinal cancer. *Surg Clin North Am.* 2000;80:1799-809.
4. Nomori H, Watanabe K, Ohtsuka T, Naruke T, Suemasu K. In vivo identification of sentinel nodes for clinical stage I non-small cell lung cancer for abbreviation of mediastinal lymph node dissection. *Lung Cancer.* 2004;46:49-55.
5. Nomori H, Horio H, Naruke T, Orikasa H, Yamazaki K, Suemasu K. Use of technetium-99m tin colloid for sentinel lymph node identification in non-small cell lung cancer. *J Thorac Cardiovasc Surg.* 2002; 124:486-92.
6. Liptay MJ, Masters GA, Winchester DJ, Edelman BL, Carrido BJ, Hirshcritt TR, et al. Intraoperative radioisotope sentinel lymph node mapping in non-small cell lung cancer. *Ann Thorac Surg.* 2000;70: 384-90.
7. Liptay MJ, Grondin SC, Fry WA, Pozdol C, Carson D, Knop C, et al. Intraoperative sentinel lymph node mapping in non-small cell lung cancer improves detection of micrometastases. *J Clin Oncol.* 2002;20: 1984-8.
8. Schmidt FE, Woltering EA, Webb WR, Garcia OM, Cohen JE, Rozans MH. Sentinel nodal assessment in patients with carcinoma of the lung. *Ann Thorac Surg.* 2002;74:870-4.
9. Melfi FM, Chella A, Menconi GF, Givigliano F, Boni G, Mariani G, et al. Intraoperative radioguided sentinel lymph node biopsy in non-small cell lung cancer. *Eur J Cardiothorac Surg.* 2003;23:214-20.
10. Sugi K, Kaneda Y, Sudoh M, Sakano H, Hamano K. Effect of radioisotope sentinel node mapping in patients with cT1 N0 M0 lung cancer. *J Thorac Cardiovasc Surg.* 2003;126:568-73.
11. Carlson GW, Murray DR, Greenlee R, Alazraki N, Fry-Spray C, Poole R, et al. Management of malignant melanoma of the head and neck using dynamic lymphoscintigraphy and gamma-probe-guided sentinel lymph node biopsy. *Arch Otolaryngol Head Neck Surg.* 2000;126: 433-7.
12. de Wilt HW, Thompson JF, Uren RF, Ka VS, Scolyer RA, McCarthy WH, et al. Correlation between preoperative lymphoscintigraphy and metastatic nodal disease sites in 362 patients with cutaneous melanoma of the head and neck. *Ann Surg.* 2004;239:544-52.
13. Albertini JJ, Cruse CW, Rapaport D, Wells K, Ross M, DeConti R, et al. Intraoperative radio-lymphoscintigraphy improves sentinel lymph node identification for patients with melanoma. *Ann Surg.* 1996;223: 217-24.
14. Ishihara T, Kaguchi A, Matsushita S, Shiraishi S, Tomiguchi S, Yamashita Y, et al. Management of sentinel lymph nodes in malignant skin tumors using dynamic lymphoscintigraphy and the single-photon-emission computed tomography/computed tomography combined system. *Int J Clin Oncol.* 2006;11:214-20.
15. Nomori H, Horio H, Naruke T, Suemasu K. What is the advantage of a thoracoscopic lobectomy over a limited thoracotomy procedure for lung cancer surgery? *Ann Thorac Surg.* 2001;72:879-84.
16. Nomori H, Ikeda K, Mori T, Kobayashi H, Iwatani K, Kawanaka K, et al. Sentinel node navigation segmentectomy for c-T1 N0 M0 non-small cell lung cancer *J Thorac Cardiovasc Surg.* 2007;133:780-5.
17. Naruke T, Suemasu K, Ishikawa S. Lymph node mapping and curability at various levels of metastasis in resected lung cancer. *J Thorac Cardiovasc Surg.* 1978;76:832-9.
18. Okada M, Yoshikawa K, Hatta T, Tsubota N. Is segmentectomy with lymph node assessment an alternative to lobectomy for non-small cell lung cancer of 2 cm or smaller? *Ann Thorac Surg.* 2001;71:956-61.
19. Yoshikawa K, Tsubota N, Kodama K, Ayabe H, Taki T, Mori T, et al. Prospective study of extended segmentectomy for small lung tumors: the final report. *Ann Thorac Surg.* 2002;73:1055-9.

GTS

Novel Germline Mutation: *EGFR* V843I in Patient With Multiple Lung Adenocarcinomas and Family Members With Lung Cancer

Koei Ikeda, MD, PhD, Hiroaki Nomori, MD, PhD, Takeshi Mori, MD, PhD, Jiichiro Sasaki, MD, PhD, and Toshiaki Kobayashi, MD, PhD

Department of Thoracic Surgery, Graduate School of Medical Sciences, Kumamoto University, Department of Respiratory Medicine, Kumamoto University Hospital, Kumamoto and Department of Assistive Diagnostic Technology, National Cancer Center Hospital, Tokyo, Japan

A novel germline transmission of the epidermal growth factor receptor (EGFR) mutation V843I in a family with multiple members with lung cancer is reported. The proband was a 70-year-old woman with multiple adenocarcinomas who exhibited secondary *EGFR* mutations, either L858R or L861Q, in the specimens of resected tumors, in addition to a germline *EGFR* V843I mutation. These observations suggest that the germline *EGFR* V843I mutation might have altered EGFR signaling in the multicentric development of adenocarcinoma, bronchoalveolar carcinoma, and atypical adenomatous hyperplasia and also might have had a role in the development of lung cancer in multiple members of her family.

(Ann Thorac Surg 2007;xx:xxx)

Recent advances in high-resolution computed tomography (CT) have increased the detection of multicentric adenocarcinoma (AD) [1]. However, the cause of multicentric development of lung AD is unknown. Recently a germline epidermal growth factor receptor (EGFR) mutation, T790M, found to be a drug-resistant mutation of EGFR tyrosine kinase inhibitors, was reported in one family that included several patients with lung cancer [2]. We report a novel germline mutation, *EGFR* V843I, in a woman with multiple lung ADs and family members with lung cancer.

The patient was a 70-year-old woman. Her father and a F1 brother (I-1 and II-1, respectively; Fig 1) had died of lung cancer. Her brother also had stomach and prostate gland cancer. In the case patient, multiple pulmonary nodules were demonstrated on CT scans obtained during a routine medical examination (Fig 2). A CT-guided needle F2 biopsy of the bilateral nodules revealed AD. Right upper and middle lobectomies were performed, followed by wedge resection of the left pulmonary nodules 2 months later. Pathologic examination revealed 3 ADs (Figs 2A–C), 4 bronchioloalveolar carcinomas (BACs) (Fig 2D), and 3 lesions of atypical adenomatous hyperplasia (AAH) (Fig 2E). The disease had metastasized to the lymph nodes of the AQ: 1 right upper lobe. We classified AD in the posterior segment of the right upper lobe (Fig 2B) as T1N1M0, stage IIA, because the nodule was the largest and the pathologic findings showed intratumoral lymphatic invasion. The other resected tumors were classified as T1N0M0, stage IA. The patient refused adjuvant chemotherapy. She has been alive without recurrence for 8 months after surgery.

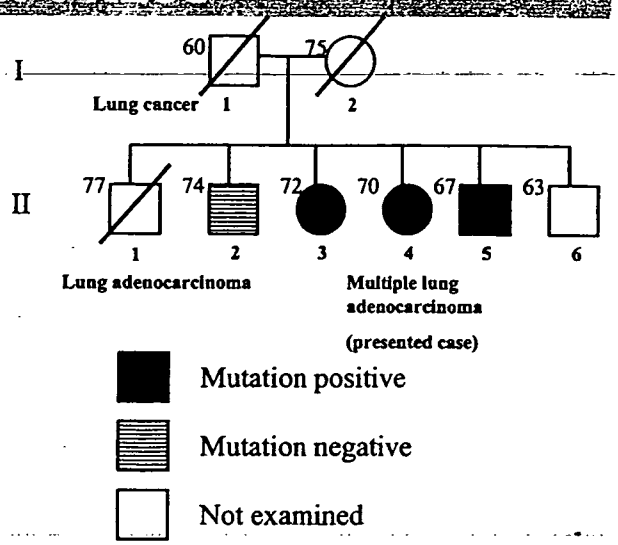

Fig 1. Pedigree of family of case patient (II-4). Boxes and circles indicate males and females, respectively; numbers at left above indicate age at death or time of mutation analysis; and oblique line shows deceased family members.

DNA extraction and direct sequencing were performed by SRL Laboratory Inc, Tokyo, Japan. DNA was extracted from formalin-fixed, paraffin-embedded specimens of three resected ADs (Figs 2A-C), one BAC (Fig 2D), and one AAH (Fig 2E). The tumor cells were microscopically dissected from their 5-μm sections for DNA extraction. Direct sequencing from *EGFR* exon 18, exon19, exon 20, and exon 21 was performed. In addition, mutation analyses were performed on resected adjacent healthy lung tissue and peripheral blood mononuclear cells. After obtaining written informed consent from family members, germline mutations in the peripheral blood mononuclear cells were analyzed in her two brothers (II-2 and II-5; Fig 1) and one sister (II-3; Fig 1), none of whom had lung cancer.

Specimens from all five tumors examined, healthy lung tissue, and peripheral blood mononuclear cells from the patient exhibited the *EGFR* V843I mutation (Figs 3A, C, and E) in exon 21 of the *EGFR* gene. In addition, *EGFR* F3 L861Q (Fig 3B) was detected in ADs in the apical segment of the right upper lobe (Fig 2A) and in the left upper lobe (Fig 2C), and *EGFR* L858R (Fig 3D) in AD in the posterior segment of the right upper lobe (Fig 2B), BAC in the lateral segment of the right middle lobe (Fig 2D), and AAH in the apical anterior segment of the left upper lobe (Fig 2E) (Table 1). These mutations were not detected in T1, AQ: 2 the healthy lung tissue and peripheral blood mononuclear cells. Of her three affected family members, two (II-3 and II-5; Fig 1) had the germline V843I mutation and one (II-2; Fig 1) did not. All mutations were harbored in exon 21 of the *EGFR* gene, and there were no mutations of exon 18, 19, or 20 in any specimens examined.

Comment

Frequent detection of the *EGFR* mutation in lung ADs with BAC features has been reported [3]. Recently, the

Accepted for publication Oct 2, 2007.

Address correspondence to Dr Nomori, Department of Thoracic Surgery, Graduate School of Medical Sciences, Kumamoto University, 1-1-1 Honjo, Kumamoto, 860-8556, Japan; e-mail: hnomori@qk9.so-net.ne.jp.

Published by Elsevier Inc

0003-4975/07/$34.00
doi:10.1016/j.athoracsur.2007.10.012

possibility of an important role of the *EGFR* mutation in the carcinogenesis of lung AD has also been suggested. Tang and colleagues [4] showed that the *EGFR* mutation is frequently present in the normal epithelium of patients with *EGFR* mutant lung AD and suggested that the *EGFR* mutation might be a very early event in the pathogenesis of lung AD. Ji and colleagues [5] demonstrated a close relationship between the *EGFR* mutation and carcinogenesis of lung AD in experiments in transgenic mice.

The *EGFR* V843I mutation has been reported in a patient with lung AD who exhibited a partial response to therapy with gefitinib (Iressa; AstraZeneca Pharmaceuticals LP, Willmington, Delaware) [6] and in a patient with bile duct AD [7]. Our case patient had a germline *EGFR* V843I mutation and additional mutations L861Q and L858R in all five tumor specimens examined. Knudson [8] proposed the two-hit theory of tumor development, that is, that tumors can develop from healthy tissue with congenital first mutations following acquisition of second mutations. We speculate that multifocal development of AD, BAC, and AAH in the case patient might have occurred as a result of second-hit mutations L861Q and L858R in the setting of a germline V843I mutation.

However, the effects of the *EGFR* V843I mutation on EGFR signaling and the molecular importance of the double mutation on *EGFR* exon 21 are unknown. The patient's father and a brother had died of lung cancer. However, another brother and a sister, each of whom had germline *EGFR* V843I mutation, have not developed lung cancer despite being almost 70 years old. The role of germline *EGFR* V843I mutation in multifocal lung carcinogenesis and the familial occurrence of lung cancer in the case patient are still unclear. In vitro experiments are

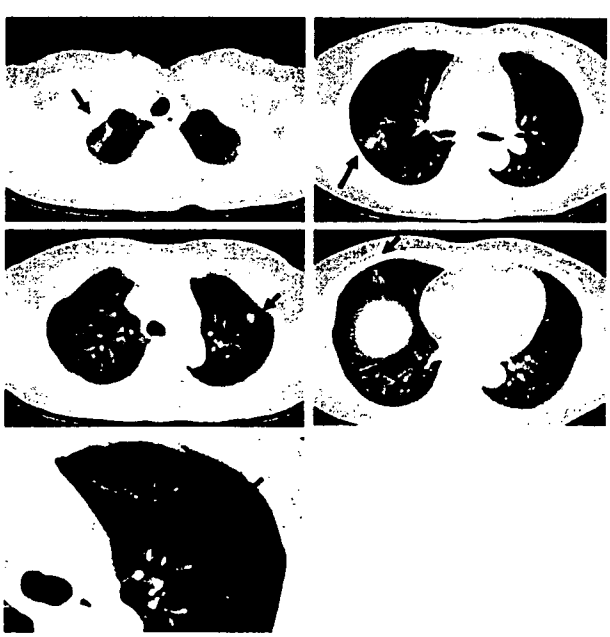

Fig 2. Findings at computed tomography. A, Adenocarcinoma (arrow) in apical segment of right upper lobe. B, Adenocarcinoma (arrow) in posterior segment of right upper lobe. C, Adenocarcinoma (arrow) in left upper lobe. D, Bronchioloalveolar carcinoma (arrow) in right middle lobe. E, Atypical adenomatous hyperplasia (arrow) in left upper lobe.

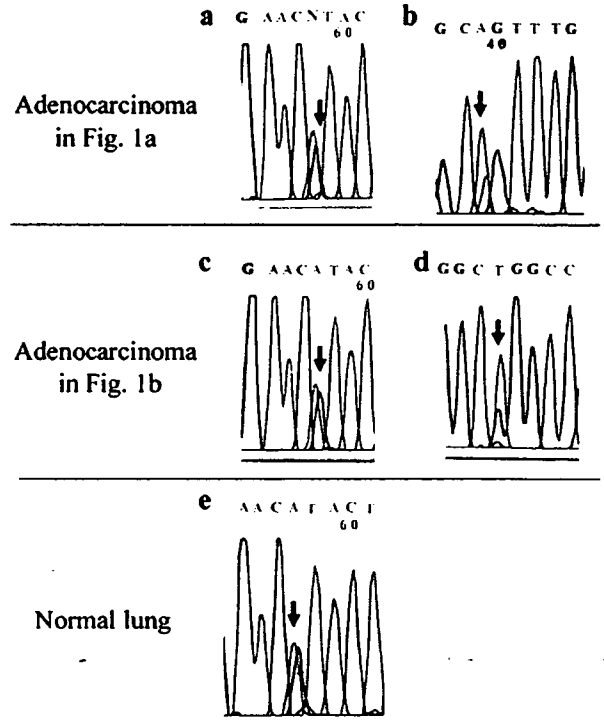

Fig 3. Nucleotide sequence tracings. Tracings A, C, and E show G to A mutation, which represents germline V843I mutation in EGFR gene. Tracing B shows A to T mutation, which represents L861Q mutation in tumor (reverse sequence). Tracing D shows T to G mutation, which represents L858R mutation in tumor (reverse sequence).

Table 1. EGFR Mutations in Examined Tumor Specimens

Pedigree Position and Specimen	EGFR Mutation 1	EGFR Mutation 2
II-4 (case patient)		
AD in S1	Exon 21 V843I	Exon 21 L861Q
AD in S2	Exon 21 V843I	Exon 21 L858R
AD in S3	Exon 21 V843I	Exon 21 L861Q
BAC in S4	Exon 21 V843I	Exon 21 L858R
AAH in S3	Exon 21 V843I	Exon 21 L858R
Healthy lung tissue	Exon 21 V843I	None
Peripheral blood cells	Exon 21 V843I	None
II-2 (brother of case patient)		
Peripheral blood cells	None	None
II-3 (sister of case patient)		
Peripheral blood cells	Exon 21 V843I	None
II-5 (brother of case patient)		
Peripheral blood cells	Exon 21 V843I	None

AD = adenocarcinoma; AAH = atypical adenomatous hyperplasia; S1 = apical segment of right upper lobe; S2 = posterior segment of right upper lobe; S3 = apical anterior segment of left upper lobe; S4 = lateral segment of right middle lobe.

needed to clarify the effects of *EGFR* V843I mutation on EGFR signaling, as is accumulation of clinical cases to determine the role of germline *EGFR* mutation in lung carcinogenesis.

References

1. Zwirewich CV, Miller RR, Muller NL. Multicentric adenocarcinoma of the lung: CT-pathologic correlation. Radiology 1990;176:185–90.
2. Bell DW, Gore I, Okimoto RA, et al. Inherited susceptibility to lung cancer may be associated with the T790M drug resistance mutation in EGFR. Nat Genet 2005;37:1315–6.
3. Blons H, Côté JF, Le Corre D, et al. Epidermal growth factor receptor mutation in lung cancer is linked to bronchioloalveolar differentiation. Am J Surg Pathol 2006;30:1309–15.
4. Tang X, Shigematsu H, Bekele N, et al. EGFR tyrosine kinase domain mutations are detected in histologically normal respiratory epithelium in lung cancer patients. Cancer Res 2005;65:7568–72.
5. Ji H, Li D, Chen L, et al. The impact of human EGFR kinase domain mutations on lung tumorigenesis and in vivo sensitivity to EGFR-targeted therapies. Cancer Cells 2006;9:485–95.
6. Shih J-Y, Gow C-H, Yu C-J, et al. Epidermal growth factor receptor mutation in needle biopsy/aspiration samples predicts response to gefitinib therapy and survival of patients with advanced non–small cell lung cancer. Int J Cancer 2006;118:963–9.
7. Leone F, Cavalloni G, Pignochino Y, et al. Somatic mutation of epidermal growth factor recepter in bile duct and gallbladder carcinoma. Clin Cancer Res 2006;12:1680–5.
8. Knudson AG Jr. Overview: genes that predispose to cancer. Mutat Res 1991;247:185–90.